Stress State Dependent Failure Loci of a Talc-filled Polypropylene Material under Static Loading and Dynamic Loading

Shaoting Lin[1,*], Yong Xia[1], Chin-Hsu Lin[2], Jingyi Wang[1], Gongyao Gu[1]

[1] Department of Automotive Engineering, Tsinghua University, Beijing 100084, China
[2] Vehicle Systems Research Laboratory, GM R&D, Michigan, USA
* Corresponding author: linst06@gmail.com

Abstract A set of stress state dependent failure loci of a talc-filled Polypropylene material under static loading and dynamic loading was obtained by using a combined experimental-numerical approach. Uniaxial tension, simple shear, notched tension and punching tests were carried out to identify fracture locus under nonnegative stress triaxiality. Corresponding finite element analysis was performed to obtain the evolution of stress triaxiality of each failure element in each type of test. Different fracture prediction techniques were applied in static loading and dynamic loading, respectively. Under dynamic loading, an average value of the stress triaxiality was identified to determine stress triaxiality of critical point during the whole loading process in each type of test. By comparing force-displacement curves from both test and modeling, equivalent plastic strain in identified stress triaxiality can be obtained. Under static loading, damage evolution rule was utilized to optimize failure locus, and quadratic function was selected to optimize fracture locus. Significant difference of fracture locus between static loading and dynamic loading was observed.

Keywords Failure locus, Stress triaxiality

1. Introduction

With the rising requirements for energy saving and environment protection, thermoplastics, as one of the lightweight materials, have been widely employed in many thin-walled components of intricate shape in the automotive industry such as in interior and exterior trims. This on the other hand drives the demand for the accurate characterization of mechanical properties like yielding criteria and failure locus for thermoplastics. Particularly, fracture of thermoplastic material is commonly observed in occupant and pedestrian impacts, and some of the purposely intended fractures are crucial for absorbing impact energy and reducing occupant injury. However, the fracture behavior of thermoplastics is multifaceted, and it is sensitive to loading speed, loading mode, temperature, etc. A number of commonly-used numerical ductile fracture models such as the constant equivalent strain criterion, the Johnson-Cook (J-C) fracture model, and the Wilkinson (W) failure mode [1] have been implemented in commercial codes such as ABAQUS, LS-DYNA and PAM-CRASH. The main drawback of these fracture models is that accurate predictions of failure can only be achieved for limited stress state and strain rate, which cannot be applied for thermoplastics. New failure model developed by Y. Bai [2] extends the Mohr-Coulomb (MC) criterion from 2D shell to 3D solid such that failure strain is a function of both stress triaxiality and Lode angle parameter. But none of these models consider the influence of strain rate on failure strain, which is crucial for capturing the fracture behavior of a thermoplastic.

A general form of the strain based facture loci [3] can be written as follows.

$$\bar{\varepsilon}_f = f(\eta) = f\left(\frac{\sigma_h}{\bar{\sigma}}\right) \tag{1}$$

where $\bar{\varepsilon}_f$ is effective plastic strain to fracture, η is stress triaxiality defined by the ratio of hydrostatic stress σ_h to equivalent stress $\bar{\sigma}$. Considering the different failure behavior under static and dynamic loading for polymeric materials, we modify the Eq. (1) to the following equations.

$$\bar{\varepsilon}_f = f(\eta) = \begin{cases} f_1(\eta),\ \eta > 0, \text{static loading} \\ f_2(\eta),\ \eta > 0, \text{dynamic loading} \end{cases} \tag{2}$$

In this paper, the main task is to give the explicit Eq. (2) of a talc-filled impact modified polypropylene (PP). An empirical fracture locus depending on the parameters of stress state under both quasi static and dynamic loading was obtained using a combined experimental-numerical identification method. Different specimen geometries were designed to carry out tests of various loading conditions including uniaxial tension, simple shear, notched tension, and punching. The stress state parameters were stress triaxiality.

The material model SAMP-1 [4] (a Semi-Analytical Model for Polymers) in LS-DYNA was utilized to obtain stress triaxiality evolution of failure element during the process of loading. Two different fracture predictive techniques were applied to obtain fracture locus under static loading and dynamic loading. Under dynamic loading, stress triaxiality during the loading process in each test was stable. Therefore, an average value of stress triaxiality was accurate enough to identify stress triaxiality of critical failure point during the whole loading process in each type of test. By comparing force-displacement curves from both test and modeling, the equivalent plastic failure strain in the identified stress triaxiality was obtained. While under static loading, stress triaxiality varied greatly during the whole loading process. Damage evolution rule was utilized to optimize failure locus. Quadratic function was selected to optimize fracture locus under static loading.

2. Methodology

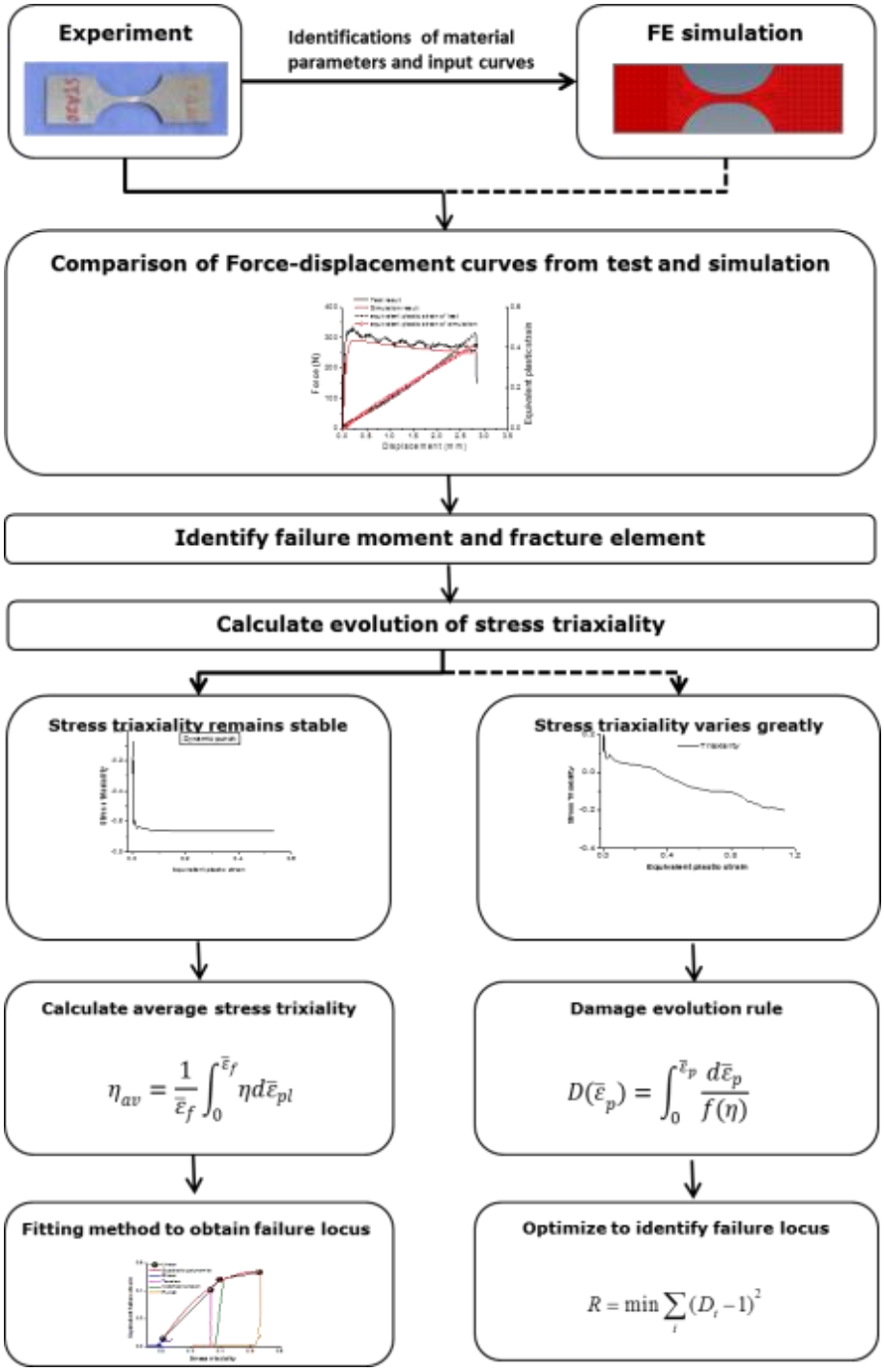

Figure 1. Procedure of identifying failure locus under static loading and dynamic loading

Bao and Wierzbicki [1, 2, 3, 5] contributed a lot on ductile failure criteria for metallic materials such as high strength steel and aluminum. Inversing engineering method was utilized to identify effective failure strain under certain stress triaxiality. Fig. 1 shows the procedure of identification of failure locus. The first step is to carry out material tests such as uniaxial tension, biaxial tension, simple shear, compression, notched-tension and punching. Basic material tests such as uniaxial tension, biaxial tension, simple shear and compression are critical for identification of material parameters and input curves, which is required in material model SAMP-1. Corresponding modeling of these tests are run to validate the material model. Also, simulations of uniaxial tension, simple shear,

notched tension and punching are run to identify equivalent failure strain under positive stress trixiality. Force-displacement curves from both test and simulation are compared to determine failure moment and extract evolution of stress triaxiality of failure element in each test. To determine stress triaxiality of critical failure point during the whole loading process, an average value of the stress triaxiality of each type of test was defined in the range from 0 to $\bar{\varepsilon}_f$

$$\eta_{av} = \frac{1}{\bar{\varepsilon}_f}\int_0^{\bar{\varepsilon}_f} \eta d\bar{\varepsilon}_{pl} \tag{3}$$

Mae [6] studied the ductile fracture locus of PP/EPR/talc Blend, using this kind of stress triaxiality approximation method as well. However, this approximation of stress triaxiality is reasonable only when stress triaxiality varies a little during the whole loading process. For polymeric materials, strain concentration is common, which leads to greatly varied stress triaxiality during the loading process especially for static loading. Y. Bai and T. Wierzbicki [2] used damage evolution rule as new popular fracture predictive technique. A linear incremental relationship was assumed here between damage indicator D and equivalent plastic strain $\bar{\varepsilon}_p$

$$D(\bar{\varepsilon}_p) = \int_0^{\bar{\varepsilon}_p} \frac{d\bar{\varepsilon}_p}{f(\eta,\bar{\theta})} \tag{4}$$

where η is stress triaxiality, $\bar{\theta}$ is lode angle parameter, and f is equivalent failure strain function. Both of the two stress direction parameters are unique functions of the equivalent plastic failure strain. A material element is considered to fail when the limit of ductility is reached, $\bar{\varepsilon}_p = \bar{\varepsilon}_f$, so that, $D(\bar{\varepsilon}_f) = 1$. In this paper, we only consider 2D fracture locus in positive stress triaxiality, thus supposing that failure strain is only dependent of stress triaxiality.

$$D(\bar{\varepsilon}_p) = \int_0^{\bar{\varepsilon}_p} \frac{d\bar{\varepsilon}_p}{f(\eta)} \ (\eta \geq 0) \tag{5}$$

To determine the explicit expression of function *f*, optimization method is required. The optimization objective function is as follows.

$$\min\{(D_T - 1)^2 + (D_S - 1)^2 + (D_N - 1)^2 + (D_P - 1)^2\} \tag{6}$$

where D_T, D_S, D_N and D_P are respectively damage indicator from tension, shear, notch tension and punch test.

Quite a few literatures show that ductile polymeric materials turn to be brittle with the increase of strain rate. Hence, in this paper, function $f(\eta)$ is studied under static loading and dynamic loading respectively. Table 1 is the test matrix for calibrating failure parameters.

Table 1. Test matrix for calibrating failure parameters

Test No.	Loading speed (m/s)	Strain rate (/s)	Stress Triaxiality range
Uniaxial tension	0.0002	0.01/s	1/3
	0.2	10/s	
Simple shear	0.0001	0.01/s	0
	0.1	10/s	
Notch tension	0.0001	0.01/s	1/3-2/3
	0.1	10/s	
Punch	0.001	/	2/3
	3.5	/	

3. Material constitutive law

A talc-filled and impact-modified polypropylene was chosen for the experimental and simulation study in this paper. All the test coupons in this paper were milled from an injecting molding plate with thickness of 3.4mm.

The material model SAMP-1 [4] in LS-DYNA developed for polymers was utilized to construct material constitutive. A quadratic form in the stress tensor is used to describe the yield surface and SAMP-1 model is restricted to isotropic formulations. The expression for the yield surface is as follows:

$$f = \sigma_{\mathrm{vm}}^2 - \mathrm{A}_0 - \mathrm{A}_1 p - \mathrm{A}_2 p^2 \leq 0 \tag{6}$$

Uniaxial tension, shear, compression and biaxial tension are four basic tests for construction of the yielding surface. Hence, all the above four tests at approximate strain rate of 0.01/s were carried out to obtain plastic true stress-strain curve as input. Fig. 2 shows equivalent stress-strain curves of four types of tests. Based on the four basic stress-strain curves, quadratic fitting formulation was selected to fit yielding surface, which is plotted in Fig. 3.

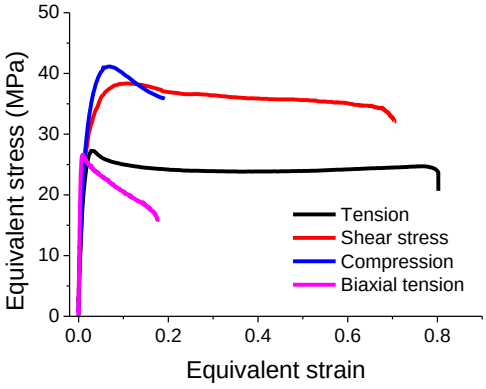

Figure 2. Input curves of SAMP-1 model

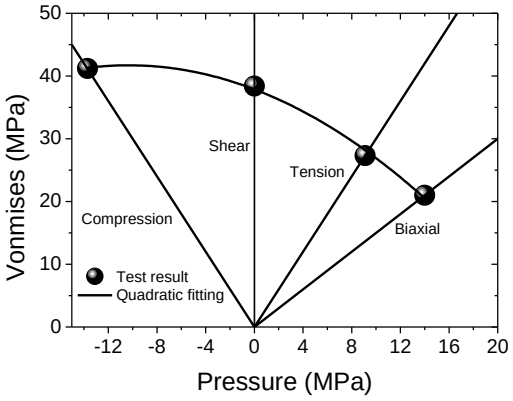

Figure 3. Yielding surface

A proper visco-plastic consideration of the rate effects is included in SAMP-1 model. In order to

characterize property of strain rate dependence of polymeric materials, multiple load curves of tension tests corresponding to different values of the plastic strain rate are input in material model. It is assumed in SAMP-1 model that strain rate effect in compression and shear is the same as the rate effect in tensile loading. However, it should be noted that this assumption may be questionable since rate effects may depend on stress state. Fig. 4 shows uniaxial tension tests at 6 strain rate of 0.01/s, 0.1/s, 1/s, 10/s, 100/s and 200/s, which were carried out in respectively at universal material test machine for quasi static test and intermediate strain rate test machine for dynamic test.

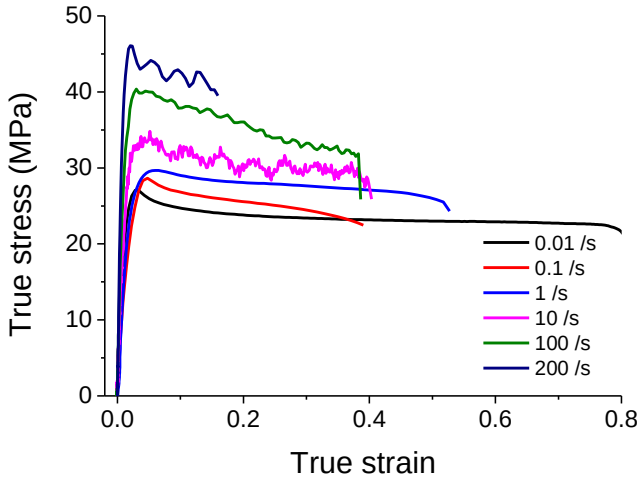

Figure 4. Uniaxial tension tests at each strain rate

4. Uniaxial tension

Fig. 5 shows specimen geometry of uniaxial tension, which was modified from the standard ASTM D638 [7]. In this paper, tension tests at strain rate of 0.01/s, 0.1/s and 1/s were carried out at universal test machine Zwick 020 and tests at strain rate of 10/s, 100/s and 200/s were conducted at intermediate strain rate hydraulic test machine. Static test set up is shown in Fig. 7 and dynamic test set up is shown in Fig. 8.

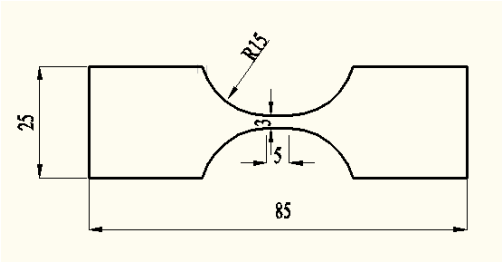

Figure 5. Schematic of tension specimen

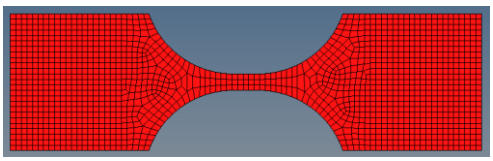

Figure 6. FEM of tension specimen

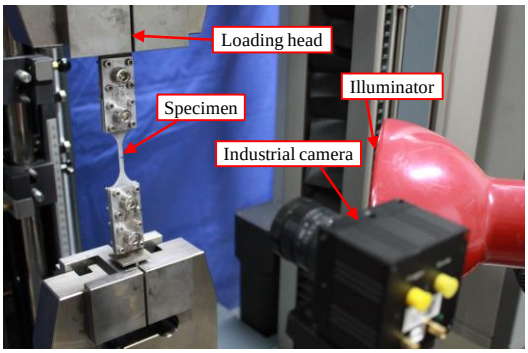

Figure 7. Test setup of quasi static test

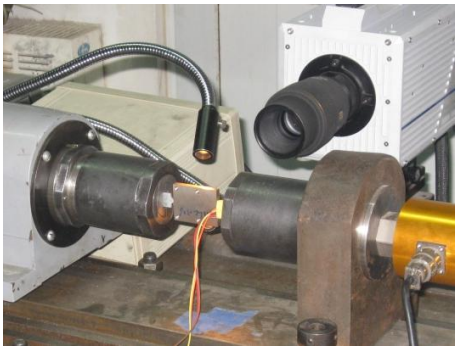

Figure 8. Test setup of dynamic test

Digital image correlation method was applied to measure the strain and displacement in gage length of tensile specimen. For force measurement, self-developed load cell (Fig. 10) was developed to measure the force signal in dynamic test. Self-developed load cell was carefully designed to avoid ringing effect which is a common problem in dynamic tests. Table 2 shows the calibration result that the linear fitting coefficient R is more than 0.9997, which indicates good consistency. In order to validate the reliability of the self-development load cell, tensile tests of LY12CZ, a commonly-known material with little strain rate effect were performed respectively at 0.5 mm/min, 5 mm/min, 1.1 m/s and 2.2 m/s and force measurements of these tests were acquired from self-developed load cell. Fig. 9 indicates no significant strain rate effect, which conforms to commonly-known mechanical property of LY12CZ. This result validates the reliability of our self-developed load cell.

Table 2. Calibration factors and correlation coefficients based on the calibration test results

Test No.	Loading speed (mm/min)	Factor (N/mV)	Correlation coefficient
1	0.2	0.539	0.9998
2	0.2	0.540	0.9998
3	0.2	0.537	0.9998
4	0.5	0.537	0.9998
5	0.5	0.533	0.9997
6	0.5	0.538	0.9998
Average value	/	0.537	/

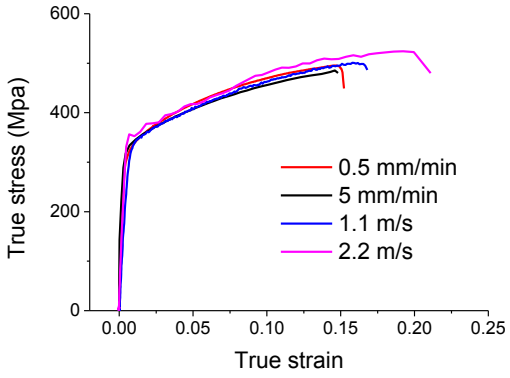

Figure 9. Tension curves at different loading speeds of LY12CZ

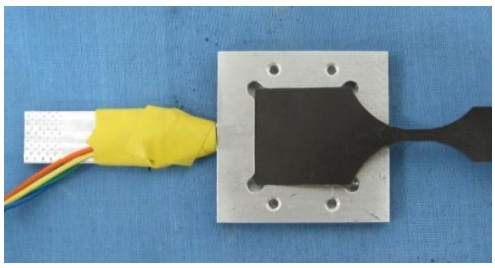

Figure 10. Self-developed load cell

In order to evaluate failure strain under tensile test, we closely investigated the tensile tests at strain rate of 0.01/s and strain rate of 10/s. For tensile test at 0.01/s, we directly obtained equivalent failure strain from test. Fig. 11 plots the force level, equivalent plastic strain and gamma (stands for the principal strain angle in radians, measure counterclockwise from the positive X-axis). Since gamma was quite close to 0, we assumed that the tensile test at 0.01/s was close to uniaxial tension stress state even though strain localization occurs after large deformation. Fig. 12 is image of specimen right before fracture and color distribution shows effective strain distribution in gage length. Via DIC method, we can acquire equivalent plastic failure strain as 0.76. Consequently, we safely identified one initial value of function $f(\eta)$ at static loading, $f(1/3) = 0.76$.

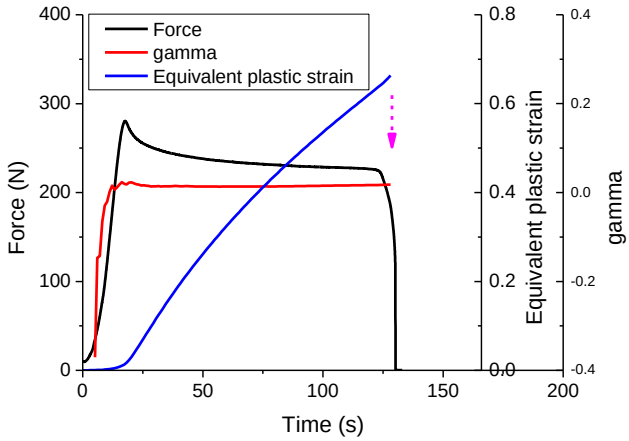

Figure 11. Equivalent strain, force and gamma coefficient, tensile test, 0.01/s

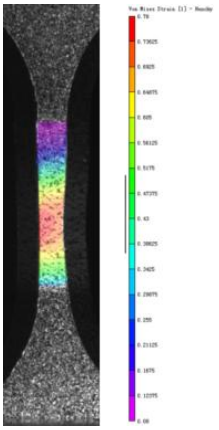

Figure 12. Strain distribution right before fracture, tension, 0.01/s

For tensile tests at 10/s, similar method can be utilized to determine fracture strain at strain rate of 10/s. Meanwhile, corresponding simulation can also help us to find the equivalent plastic failure strain and validate our test result. Simulation model was with 1mm shell element which is shown in Fig. 6. All the tensile curves under 6 strain rates, compression, shear and biaxial curves at lowest strain rate of 0.01/s were input in SAMP-1. Fig. 13 shows good correlation between simulation and test. By comparing force-displacement curves from both test and simulation, stress triaxiality evolution curve of failure element was obtained, which is shown in Fig. 14. From Fig.14, we can observe that stress triaxiality is close to 0.33, which indicates an ideal uniaxial tensile state. Since stress triaxiality at 10/s was stable, average value of stress triaxiality was calculated according to Eq. (3), $f(0.33) = 0.41$.

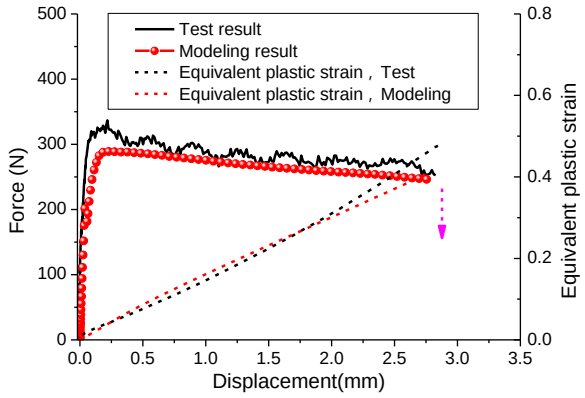

Figure 13. Comparison curves between simulation and test, tension, 10/s

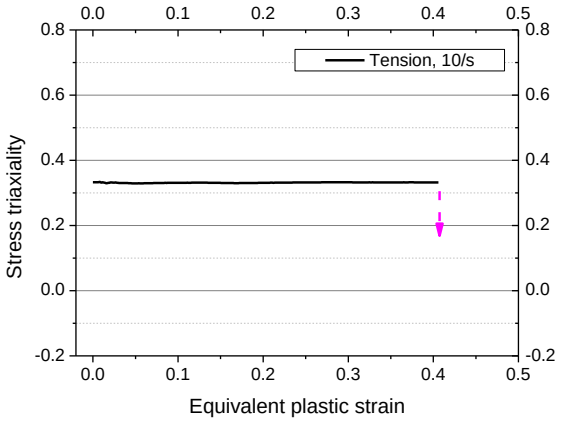

Figure 14. Stress triaxiality evolution curve, tension, 10/s

5. Simple shear

Figure 15 shows the specimen geometry of shear tests, which was similar to the design in H. Daiyan's paper [8] based on V-notched Beam standard (ASTM D 5379 [9]). Similar to tensile tests, static shear test was conducted in universal test machine with self-developed test fixture. While for dynamic shear test, similar self-developed load cell was designed to obtain force signal. Fig. 17 and Fig.18 respectively show test setup of quasi static test and dynamic test.

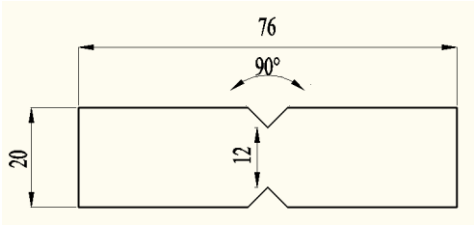

Figure 15. Schematic of shear specimen

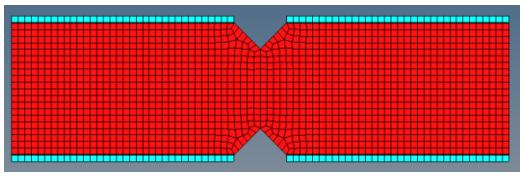

Figure 16. FEM of shear specimen

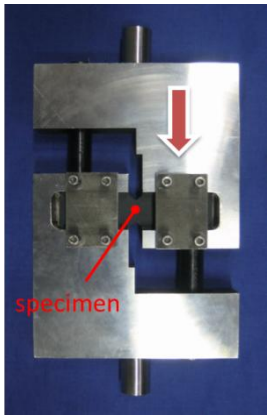

Figure 17. Test setup of quasi static test

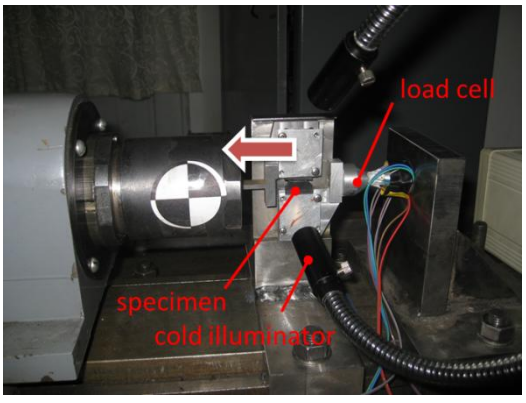

Figure 18. Test setup of dynamic test

Corresponding simulations of shear test were conducted to obtain the stress triaxiality evolution curve of failure element. Fig. 16 is the corresponding finite element model of shear specimen with 1 mm solid element. Fig. 19 and Fig. 21 shows the comparison results between simulation result and test

result respectively at 0.01/s and 10/s. By comparing the force-displacement curves of test and simulation, we identified the failure moment and obtained the stress triaxiality evolution curve of failure element. Fig. 20 and Fig.22 shows the stress triaxiality evolution curves respectively at 0.01/s and at 10/s.

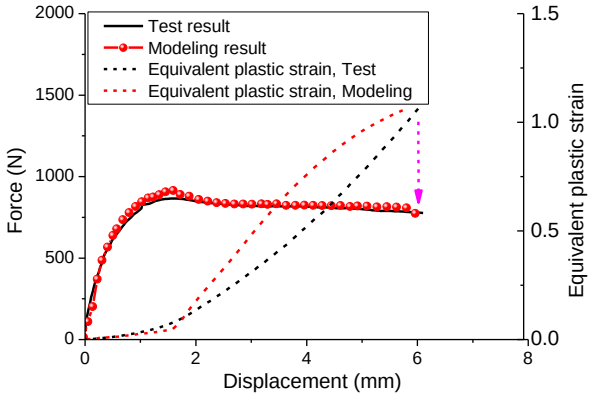

Figure 19. Comparison curves between simulation and test, shear, 0.01/s

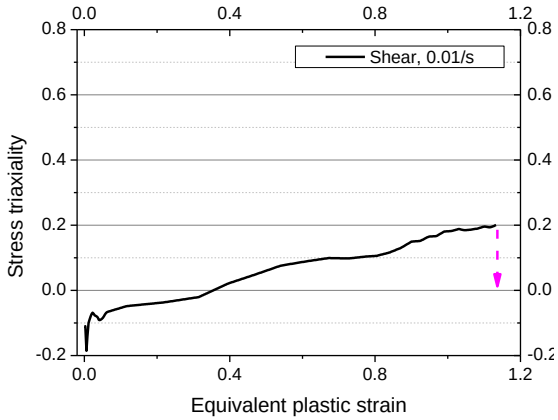

Figure 20. Stress triaxiality evolution curve, shear, 0.01/s

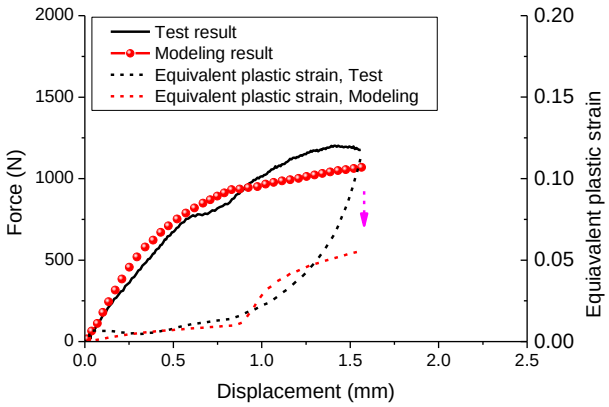

Figure 21. Comparison curves between simulation and test, shear, 10/s

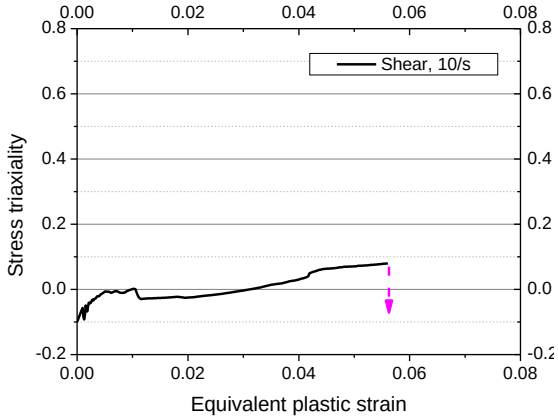

Figure 22. Stress triaxiality evolution curve, shear, 10/s

6. Notched tension

Notched tension tests were carried out to determine failure strain in stress state between uniaxial tension and biaxial tension. Fig. 23 shows schematic of notched tension specimen. Corresponding finite element model was constructed with 0.4 mm solid element, which is shown in Fig. 24. To save computation time, only half of the model was constructed.

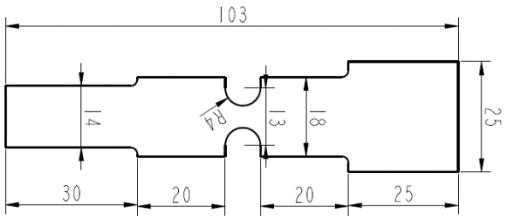

Figure 23. Schematic of notched tension specimen

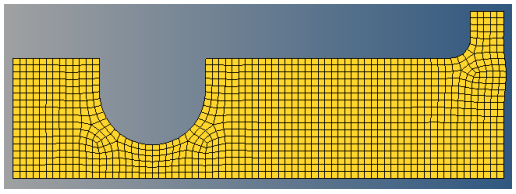

Figure 24. FEM of notched tension

Both test method and modeling technique were similar to tensile and shear test. Fig. 25 and Fig. 27 shows the comparison results between simulation result and test result respectively at 0.01/s and 10/s. Fig. 26 and Fig.28 shows the stress triaxiality evolution curves of failure element respectively at 0.01/s and at 10/s.

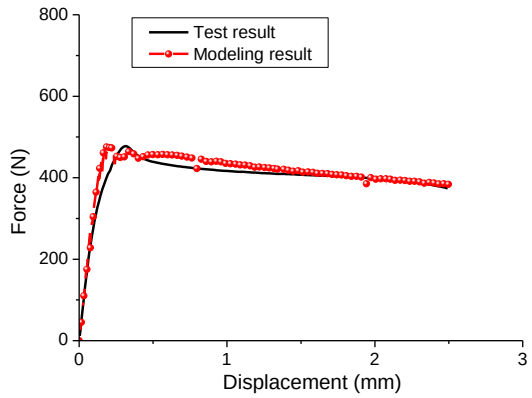

Figure 25. Comparison curves between simulation and test, notched tension, 0.01/s

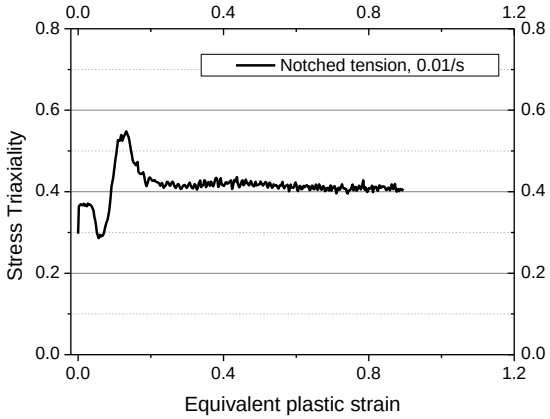

Figure 26. Stress triaxiality evolution curve, notched tension, 0.01/s

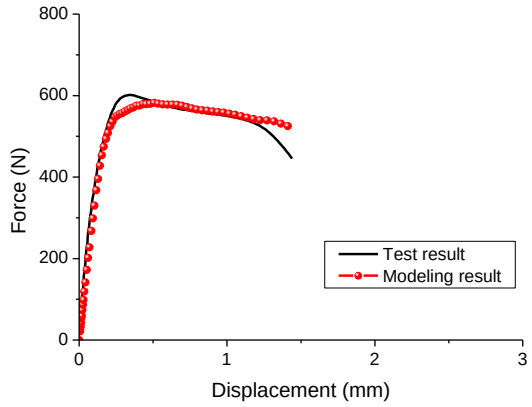

Figure 27. Comparison curves between simulation and test, notched tension, 10/s

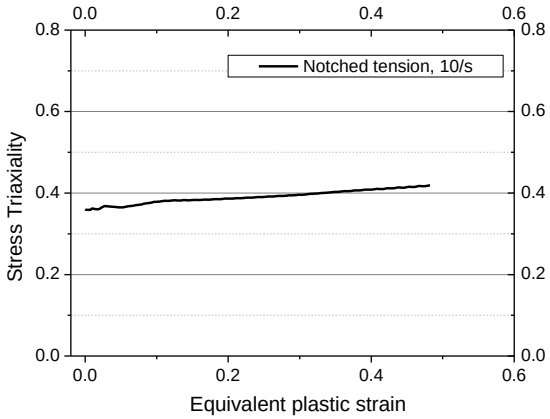

Figure 28. Stress triaxiality evolution curve, notched tension, 10/s

7. Punch

Since dominate stress triaxiality during punching loading is approximately around 0.67, punching test is used to calibrate failure locus at large stress triaxiality. The schematic of specimen for punching

tests shown in Fig. 29 mainly follows the standard of ASTM D3763 [10]. There are eight holes uniformly distributing around the outer edges of each specimen, which are used to constrain the specimen to the fixtures. Fig. 30 shows the finite element model of punch. Similarly, only quarter of the whole coupon was constructed to save computational time. Since large deformation occurred in the center region, we used fine shell element of 0.1 mm to mesh the center region.

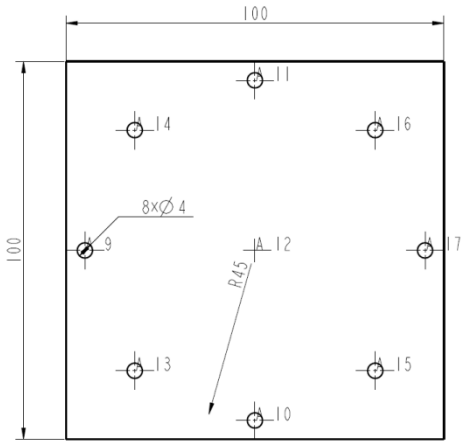

Figure 29. Schematic of punching specimen

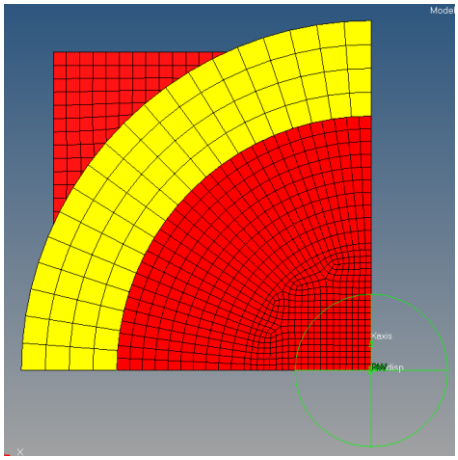

Figure 30. FEM of punch

Fig. 31 and Fig. 33 shows the comparison results between simulation result and test result respectively at 0.01/s and 10/s. Fig. 32 and Fig.34 shows the stress triaxiality evolution curves of failure element respectively at 0.01/s and at 10/s.

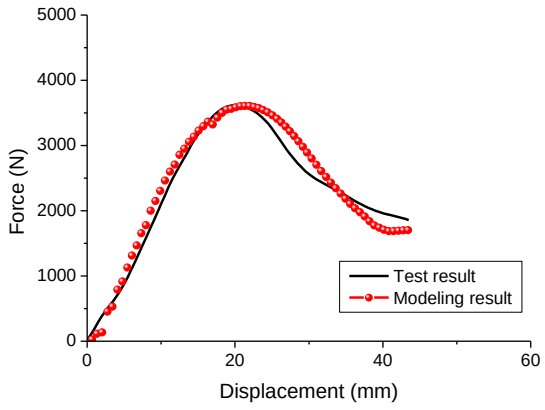

Figure 31. Comparison curves between simulation and test, punch, 0.001 m/s

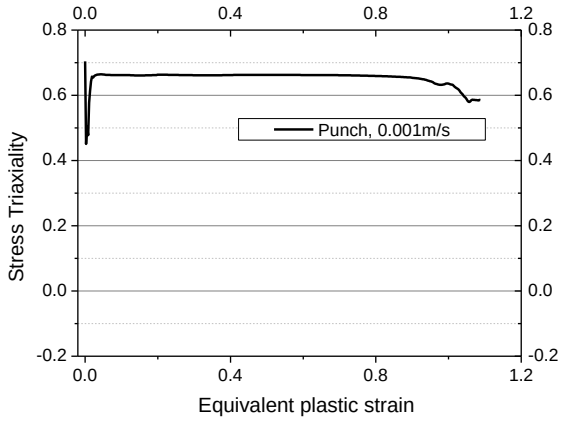

Figure 32. Stress triaxiality evolution curve, punch, 0.001 m/s

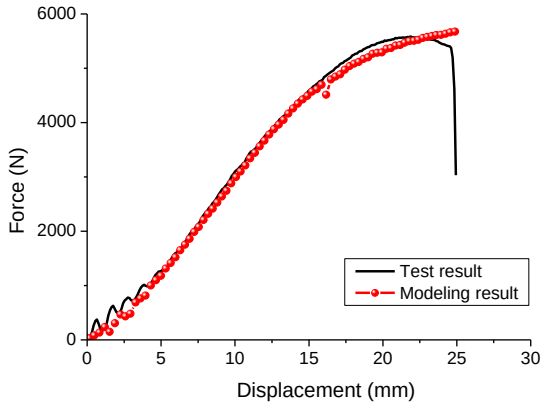

Figure 33. Comparison curves between simulation and test, punch, 3.5 m/s

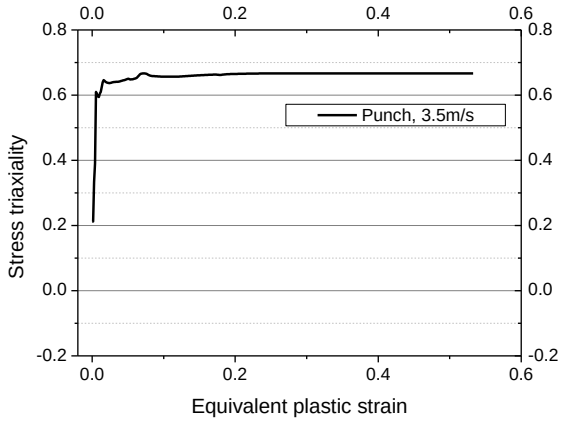

Figure 34. Stress triaxiality evolution curve, punch, 3.5 m/s

8. Construction of ductile failure criteria

8.1. Failure locus under static loading

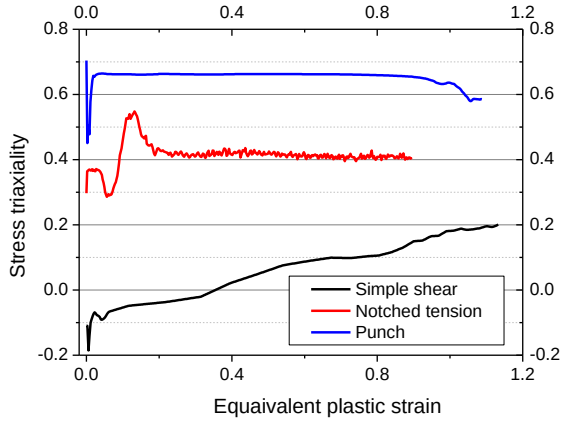

Figure 35. Stress triaxiality evolution at 0.01/s

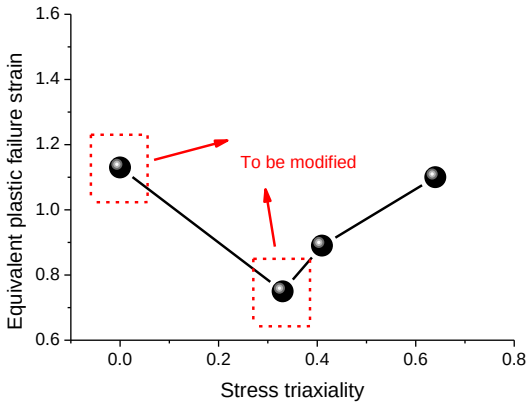

Figure 36. Failure locus from average stress triaxiality at 0.01/s

Figure 35 shows stress triaxiality evolution curves of shear, notched tension and punch under static loading. Using average stress triaxiality, we can obtain failure locus at 0.01/s shown in Fig. 36. However, since stress triaxiality varies greatly during the whole loading process in shear test, equivalent failure strain at stress triaxiality of 0 is not accurate enough. Besides, since we directly obtained equivalent failure from test via digital image correlation method in tensile test, equivalent failure strain at stress triaxiality of 0.33 is questionable as well. Therefore, damage evolution rule was used to optimize failure locus under static loading. We selected quadratic function (Eq. (7)) as optimization function. The reason we selected quadratic function partly referred to acquired four failure points in Fig. 36. Table 2 summarizes existing functions used to fitting failure locus in the equivalent strain and stress triaxiality space. And most of them are for metallic materials [3].

$$f(\eta) = B_0 + B_1\eta + B_2\eta^2 \tag{7}$$

Table 2. Equivalent failure strain, Average stress triaxiality

	Function of $f(\eta)$
Linear function	$f(\eta) = C_1\eta + C_2$

Rice-Tracey failure criteria	$f(\eta) = C_1 e^{c_2 \eta} + C_3$
Hydrostatic Stress failure criteria	$f(\eta) = \frac{C_4}{\eta}$
Power function	$f(\eta) = \eta^{C_5}$

Initial values of B_0, B_1 and B_2 were determined from acquired four points in Fig. 36. The final values of B_0, B_1 and B_2 were determined by minimizing residue R defined by Eq. (8).

$$R = (D_s - 1)^2 + (D_n - 1)^2 + (D_p - 1)^2 \quad (8)$$

Where D_s, D_n, D_p respectively stand for damage indicator in shear, notch tension and punch. Table 3 summarizes initial values and final values of coefficients B_0, B_1 and B_2. Table 4 gives values of each coefficient after optimization. Fig. 37 plots the two failure locus respectively from average stress triaxiality and from damage evolution rule. From these two comparative curves, failure strains under shear and uniaxial tension are increased after modification with optimization method.

Table 3. Initial values and final values of coefficientsB_0, B_1 and B_2

	B_0	B_1	B_2
initial values	1.12	-1.97	3.04
final values	1.22	-2.05	2.96

Table 4. Coefficients after optimization

R	D_s	D_n	D_p
0.0019	1.0192	1.0083	0.9614

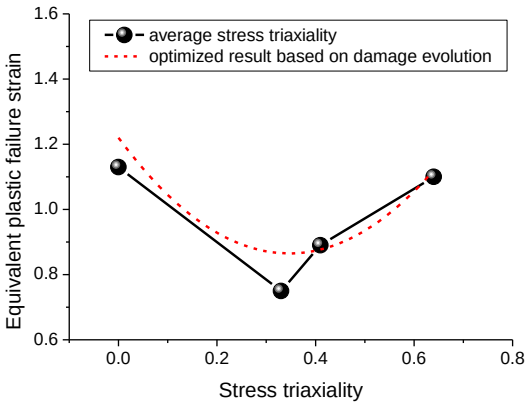

Figure 37. Failure locus from average stress triaxiality and from damage evolution rule

8.2. Failure locus under dynamic loading

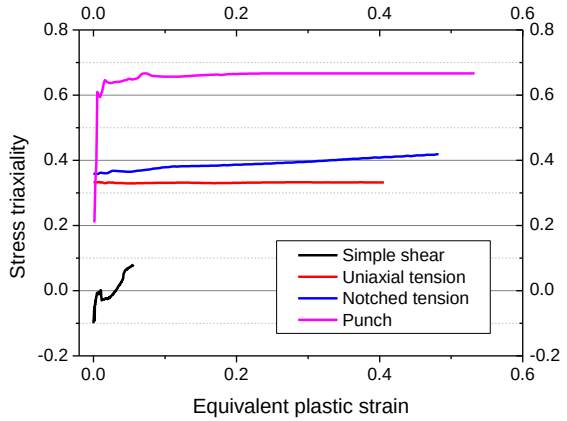

Figure 38. Stress triaxiality evolution at 10/s

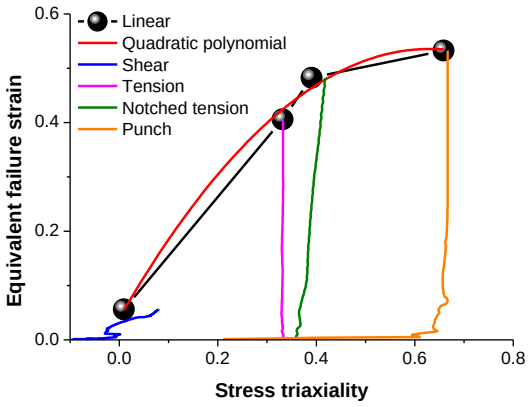

Figure 39. Failure locus at 10/s

Figure 38 shows stress triaxiality evolution curves of shear, tension, notched tension and punch under dynamic loading. We can observe that stress triaxiality of each test remains stable during loading process. Thus we can directly use the average value of stress triaxiality of each type of test. Calculation of stress triaxiality is referred to average stress triaxiality formulation Eq. (3). Table 5 summarizes the result of each test.

Table 5. Equivalent failure strain, Average stress triaxiality

Test type	Shear	Tension	Notched-tension	Punch
Average stress triaxiality	0.01	0.33	0.39	0.66
Equivalent failure strain	0.056	0.406	0.482	0.532

Quadratic polynomial fitting of four base points is plotted in Fig. 39.

9. Conclusions and Discussions

Consequently, we obtained failure locus in the space of equivalent plastic failure strain and stress triaxiality under static loading and dynamic loading. From Fig. 40, we can observe significant different failure locus between static loading and dynamic loading.

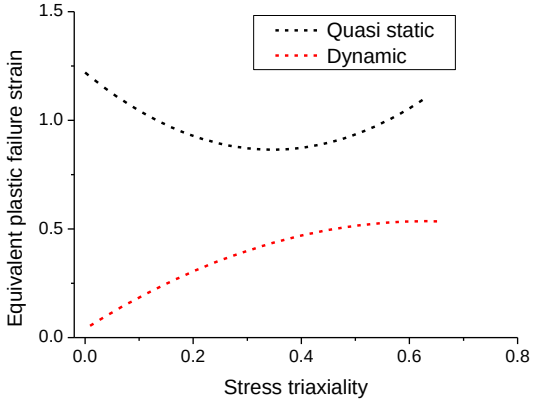

Figure 40. Failure locus under static loading and dynamic loading

We used combined experiment-numerical method to obtain failure locus in the equivalent failure strain and stress triaxiality space respectively under static loading and dynamic loading. There is significant difference between static loading and dynamic loading, which indicates strain rate impacts greatly on failure locus of the polymeric materials we studied. We utilized two failure predictive techniques to identify failure locus, trying to obtain accurate result. Under dynamic loading, average stress triaxiality method is enough determine failure locus in each type of test. While under static loading, damage evolution rule should be used to optimize the fracture locus since stress triaxiality varies greatly during the loading process especially for shear test.

10. References

[1] T. Wierzbicki, Y. Bao, Y. W. Lee, Y. Bai, Calibration and evaluation of seven fracture models. International Journal of Mechanical Sciences, 2005, 47: 719-743.
[2] Y. Bai, T. Wierzbicki, Application of extended Mohr-Coulomb criterion to ductile fracture. International Journal of Fracture, 2010, 161: 1-20.
[3] Y. Bao, T. Wierzbicki, On fracture locus in the equivalent strain and stress triaxiality space. International Journal of Mechanical Sciences, 2004, 46: 81-98.
[4] S. Kolling, A. Haufe, M. Feucht & P.A. Du Bois, SAMP-1: A Semi-Analytical Model for the Simulation of Polymers, Anwenderforum, Bamberg 2005.
[5] Y. Bao, Prediction of Ductile Crack Formulation in Uncracked Bodies. MIT PHD thesis, 2003.
[6] H. Mae, Characterization of Material Ductility of PP/EPR/talc Blend under Wide Range of Stress Triaxiality at Intermediate and High strain Rates. Journal of Applied Polymer Science, 2009, 111: 854-868.
[7] ASTM D638M, Standard test method for tensile properties of plastics, 1993.
[8] H. Daiyan, E. Andreassen, F. Grytten, H. Osnes, R.H. Gaarder, Shear testing of polypropylene materials analysed by digital image correlation and numerical simulations. Experimental Mechanics, 2012, DOI 10.1007/s11340-012-9591-7.
[9] ASTM D5379, Standard Test Method for Shear Properties of Composite Materials by the V-Notched Beam Method, 1993.
[10] ASTM D3763-95a, Standard Test Method for High Speed Puncture Properties of Plastics Using Load and Displacement Sensors, 1993.

Acknowledgements

The authors would like to thank General Motor R&D for the support on Project *Testing and Modeling of Polymeric Materials for Crash Safety CAE*. Thanks also to Foundation of Zhejiang Province Automobile Safety Technology Laboratory.